An Overview of Progressive Collapse Behavior of Steel Beam-to-Column Connections

Iman Faridmehr [1] and Mohammad Hajmohammadian Baghban [2,*]

[1]   South Ural State University, Lenin Prospect 76, Russian Federation, 454080 Chelyabinsk, Russia; imanfaridmehr@gau.edu.tr

[2]   Department of Manufacturing and Civil Engineering, Norwegian University of Science and Technology (NTNU), 2815 Gjovik, Norway

[*]   Correspondence: mohammad.baghban@ntnu.no; Tel.: +47-48-351-726

Abstract: Local failure of one or more components due to abnormal loading can induce the progressive collapse of a building structure. In this study, by the aid of available full-scale test results on double-span systems subjected to the middle column loss scenario, an extensive parametric study was performed to investigate the effects of different design parameters on progressive collapse performance of beam-to-column connections, i.e., beam span-to-depth ratio, catenary mechanism, and connection robustness. The selected full-scale double-span assemblies consisted of fully rigid (welded flange-welded web, SidePlate), semi-rigid (flush end-plate, extended end-plate), and flexible connections (top and seat angle, web cleat). The test results, including load-deformation responses, development of the catenary mechanism, and connection robustness, are presented in detail. The finding of this research further enables a comprehensive comparison between different types of steel beam-to-column connections since the effects of span-to-depth ratio and beam sections were filtered out.

Keywords: progressive collapse; steel beam-to-column connections; catenary mechanism; double-span assemblies; stiffness degradation

1. Introduction

Progressive collapse refers to a devastating phenomenon in which failure of one key structural component, due to abnormal events, leads to chain reaction and spreads to other structural members, causing disproportionate or even entire collapse of the structure [1]. Vehicle impact, terrorist attack, and gas explosions are among incidents that can produce progressive collapse in structures. By the growth of tall and complex structures throughout the world and the increasing number of terrorist- or accident-induced catastrophic events, progressive collapse has received extensive attention from scientists and structural engineers in recent decades [2–7]. The vast majority of structural design codes provide general mitigation strategies to deal with the effects of progressive collapse on structural components that may experience a relatively high demand capacity ratio (DRC).

The design of structures to resist against progressive collapse was first introduced by the UK construction regulations [8] in the aftermath of the Ronan Point building collapse in 1968. Many research and scientific efforts were concerned with this phenomenon, especially after the 9/11 terrorist attack on the World Trade Center in the US. Several design codes including general service administration (GSA) [9] and department of defense (DoD) [10] proposed the alternate load path method as an important design measure to mitigate progressive collapse. In this technique, the structural component is allowed to experience local damage when subjected to extreme loading events. However, it seeks to afford alternate paths so the damage will be localized without spreading to the surrounding areas.

During sudden column removal from the frame, high attention should be paid to the load-carrying capacity of the double-span assembly above the removed column since it has an essential function in the progressive collapse prevention. Generally, as the middle column becomes ineffectual, the catenary action develops in connected beams and slabs, leading to large deformation in beam-to-column connections. Since the robustness of connections preserves the integrity in a double-span column removal scenario, there is a necessity to investigate the beam-to-column connection performance under the simultaneous presence of moment, shear, and tension in conjunction with high ductility demand. Such a complex loading protocol negatively affects beam-to-column connection performance and poses the risk of unexpected brittle failure.

In steel structures with fully rigid and semi-rigid beam-to-column connections, the catenary mechanism plays a major role to resist progressive collapse through the axial tension in the connected beams. In fact, the catenary mechanism is the fundamental resistance source of structures to vertical loads in the large deformation stage. Beam-to-column connections with appropriate robustness and reliable axial resistance are compulsory for developing the catenary actions where this stage is the final line of defense against progressive collapse. F Wang et al. investigated the behavior of bolted and welded flange plate connections subjected to progressive collapse [11]. They concluded that the connection with welded flange plates can lead to greater flexural strength than that with bolted angles and the application of welded haunch plates can arrest fracture failure on the welds within the beam-column joint. Hao Wang et al. performed experimental tests of steel frames with different beam-column connections under falling debris impact [12]. They concluded that the majority of the external work applied to the system was absorbed by bending deformation, especially by the plastic rotation at mid-span of the beam. Besides, they concluded that the catenary action was shown to significantly improve the load-carrying capacity and energy absorption in specimens with high levels of rotational ductility. Alrubaidi et al. investigated the behavior of different steel intermediate moment frame connections under a column-loss scenario [13]. Performance of different connections was compared based on their modes of failure and load-displacement response in both flexural and catenary action stages. They concluded that significant axial tensile forces were generated in the beams and the catenary action stage was then fully mobilized, providing an increase in the progressive collapse resistance.

It has been well documented that beam-to-column connections play a vital function in mitigating progressive collapse potentials in steel structures. There is a large volume of published studies investigating the connection performances under sudden column removal, where flexible, semi-rigid [14–18], and rigid [19–22] connections have been studied in detail.

The connected beam's axial forces significantly contribute to the development of the catenary mechanism. In the case that a double-span assembly experiences large deformation, the beam-span-to-depth ratio, R_i, is also a major parameter that has been studied by several researchers [23–25]. The effect of the R_i ratio on the mitigation of progressive collapse in steel moment frames was investigated by Rezvani et al. [26]. They concluded that the vertical resistance of frames increases as the R_i ratio decreases.

A large and growing body of literature has also investigated the robustness effects of steel beam-to-column connections to mitigate the progressive collapse [27–30]. More recently, several attempts have been made to investigate the influence of the seismic design of beam-to-column connections on an anti-progressive collapse mechanism [23,31,32]. The behavior of welded unreinforced flange-bolted web and reduced beam section connections subjected to column removal were investigated by Chen et al. [33]. Using an experimental test, Yang and Tan investigated the performance of flexible and semi-rigid connections including different types of bolted beam-to-column connections [34]. They concluded that maximum tensile resistance of the connection significantly contributes to the development of catenary action after large rotations. Driver et al. [35] reported experimental results of several shear connections including 15 bolted single-angle and 6 double-angle specimens subjected to double-span assembly. They came to the conclusion that rupture or tearing of the cross-section in the

vicinity of the angle heel leads to sudden failure. Qin et al. investigated the progressive collapse behavior of conventional and reinforced welded flange-bolted web connections using numerical simulations validated by experimental tests [36]. Their study confirmed that the reinforced flange-bolted connection possesses higher ductility and robustness compared to the conventional connection, leading to more reliable collapse performance. Many researchers, such as Oosterhof and Drive [37] and Shen and Astaneh [38], have established or implemented several mechanical spring techniques for bolted-angle beam-to-column connections. Stylianidis and Nethercot [39] investigated the progressive collapse performance by using component-based connection models.

Overall, the previous literature is mainly concerned with the anti-progressive collapse behavior of typical beam-to-column connections using experimental tests or numerical simulations. However, the comprehensive comparisons of common practice beam-to-column connection performance subjected to column removal addressing the load transfer mechanisms requires robustness and ductility, and R_i effects are still very limited. Therefore, this research comprehensively investigates the anti-collapse behavior of double-span assemblies with flexible, semi-rigid, and fully rigid beam-to-column connections. This is done with the aid of available test results on steel beam-to-column connections including top-seat angle and welded unreinforced flange-bolted web. Meanwhile, for a reliable comparison of different types of double-span assemblies and to evaluate the anti-collapse performance of steel beam-to-column connections, the vertical pushdown load and equivalent rotation were normalized against connected beams' plastic hinge and plastic rotation, respectively.

2. R_i Effects on Progressive Collapse

To evaluate the effects of the R_i ratio, one set of pushdown analyses was performed in this research using structural analysis program (SAP) 2000 academic version 21. In this case study, three steel double-span assemblies with R_i ratios of 5, 10, and 15 were considered. All specimens possess fully rigid connections which were designed according to the strong column–weak beam theory in compliance with The American. Institute of Steel Construction (AISC) seismic design [40]. Figure 1 shows the topology of one studied frame with double-span assemblies.
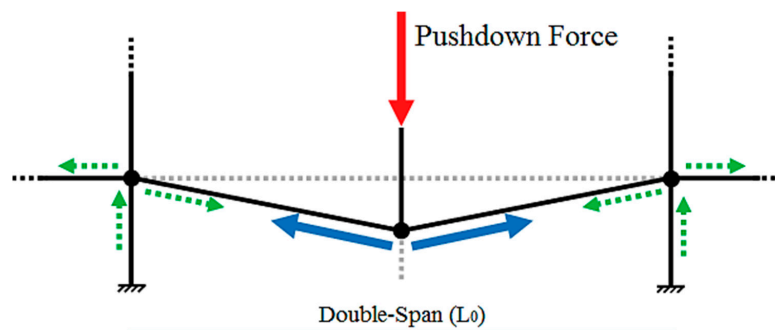

Figure 1. Double-span assembly.

In Figure 1, the pushdown force, *F*, represents the concentrated load in the pushdown analysis applied at the top of the removed column. This concentrated load is equivalent to the progressive collapse resistance of the double-span assembly. Table 1 shows the beam and column section properties used in progressive collapse analysis.

The plastic hinge capacity of connected beams, F_p, of double-span assembly can be calculated from the following equation:

$$F_p = \frac{2 M_p}{\frac{L_0}{2}} = \frac{4 W_p f_y}{L_0} \tag{1}$$

where M_p is the plastic moment of the connected beam, L_0 is the double-span assembly length, W_p is the plastic modulus of the connected beam, and f_y is the yield stress.

Table 1. Beam and Column Sections of the Steel Double-Span Assemblies (AISC Database).

Span-to-Depth Ratio, R_i	Beam Section	Column Section
5	W 40 × 149	W 40 × 531
10	W 21 × 50	W 21 × 248
15	W 12 × 35	W 12 × 50

To facilitate the comparison of different types of double-span assemblies against each other independently and regardless of connected beam plastic capacity, the pushdown force, *F*, should be normalized against the plastic hinge capacity of connected beams, F_p, as in the following equation:

$$\frac{F}{F_p} = \frac{F\, L_0}{4\, W_p\, f_y} \tag{2}$$

Besides, to highlight the differences of different beam sections during the development of the catenary action, it is necessary to normalize the chord rotation, θ, over the plastic rotation, θ_p, based on the following equations:

$$\theta = \frac{\delta}{L_0} \tag{3}$$

$$\theta_p = \frac{\delta_p}{\frac{L_0}{2}} = \frac{F_p\, 2}{K_e\, L_0} = \frac{\frac{4\, W_p\, f_y}{L_0}}{\frac{48\, E\, I_b}{L_0{}^3}}\frac{2}{L_0} = \frac{W_p\, f_y\, L_0}{6\, E\, I_b} \tag{4}$$

where I_b is the moment of inertia of a connected beam, and K_e is the elastic stiffness of a simply supported beam subjected to pushdown force. Figure 2 shows the plots of the pushdown analysis results of double-span assemblies with different R_i ratio, in which the vertical and horizontal axes are the normalized force, $\frac{F}{F_p}$, and the normalized rotation, θ/θ_p, respectively. Figure 2 shows that the frame with the larger R_i has a higher capacity to develop progressive collapse resistance. Also, the double-span assembly with the larger R_i possesses relatively high initial stiffness.
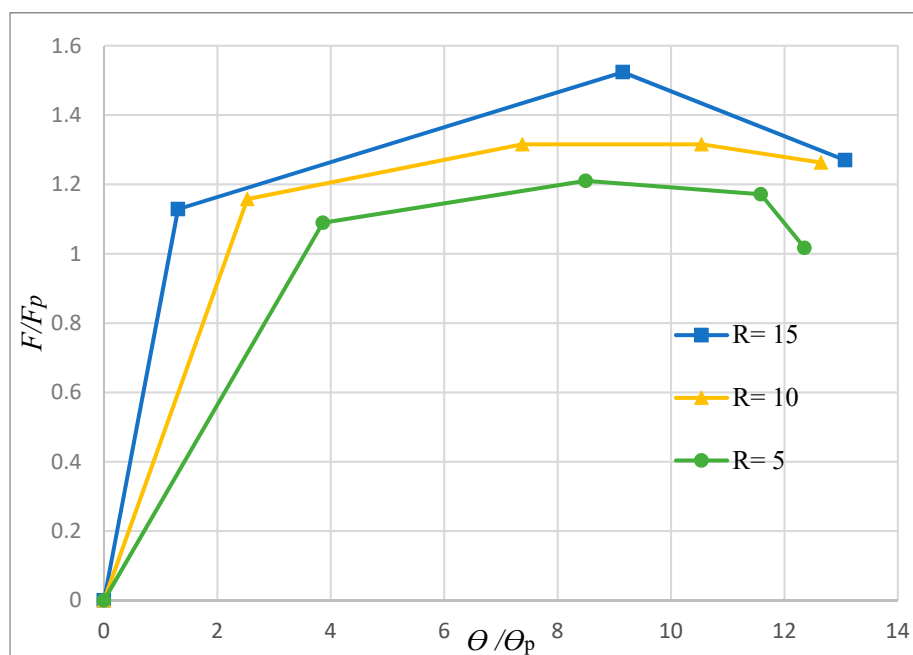

Figure 2. Normalized resistance against normalized rotation.

3. Development of Data Bank

Having recognized that different beam-to-column connections have different behavior and pushdown resistance capacity, especially the catenary mechanism, it is necessary to develop a database of test results. In this section, with the aid of available full-scale test results on double-span assemblies, this is comprehensively investigated in the performance of different steel beam-to-column connections against progressive collapse. The specimens consist of fully rigid (welded flange-welded web, SidePlate), semi-rigid (flush end-plate, extended end-plate), and flexible connections (top and seat angle, web cleat). Figure 3 depicts the configuration and geometric details of the studied connections.
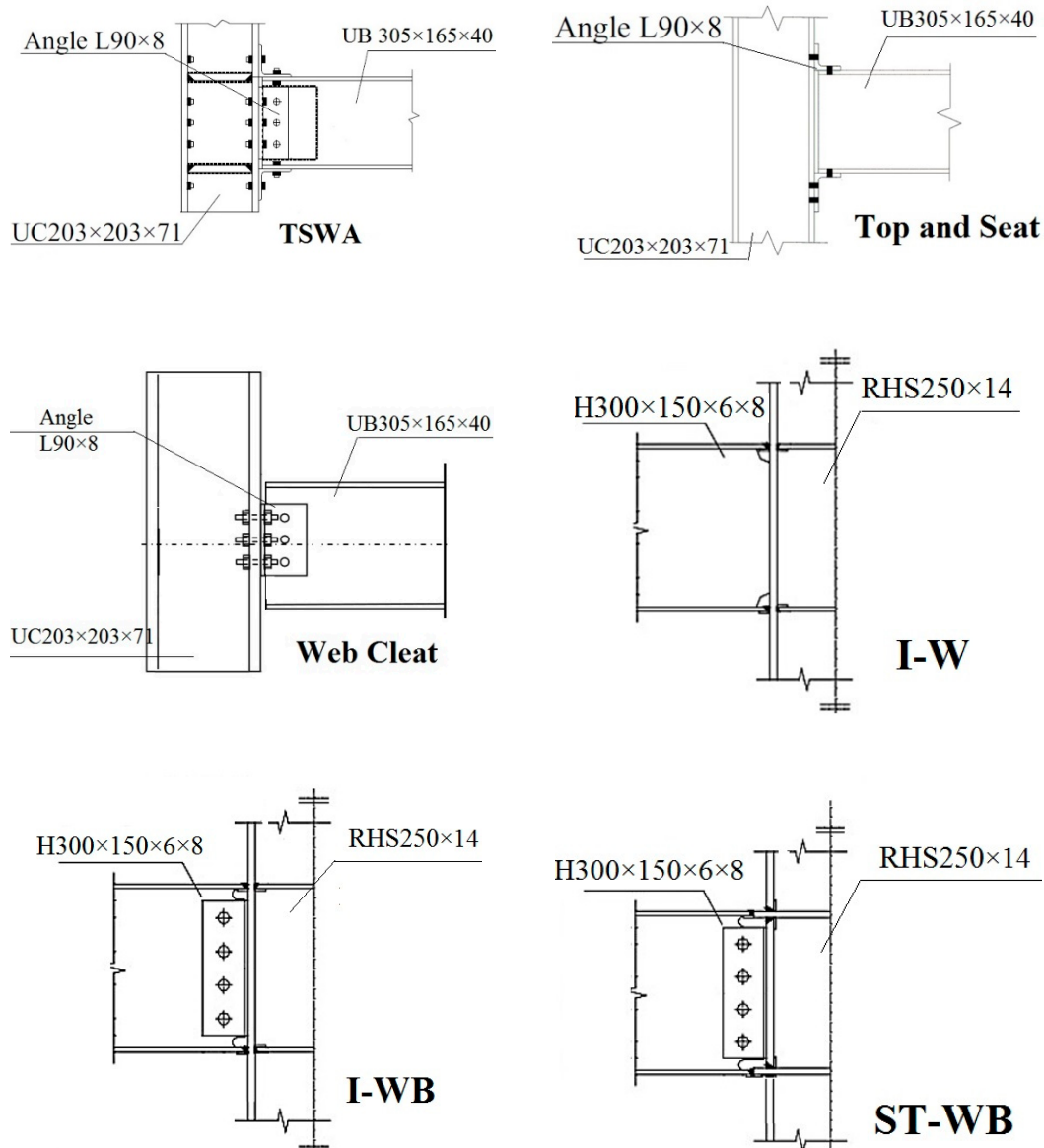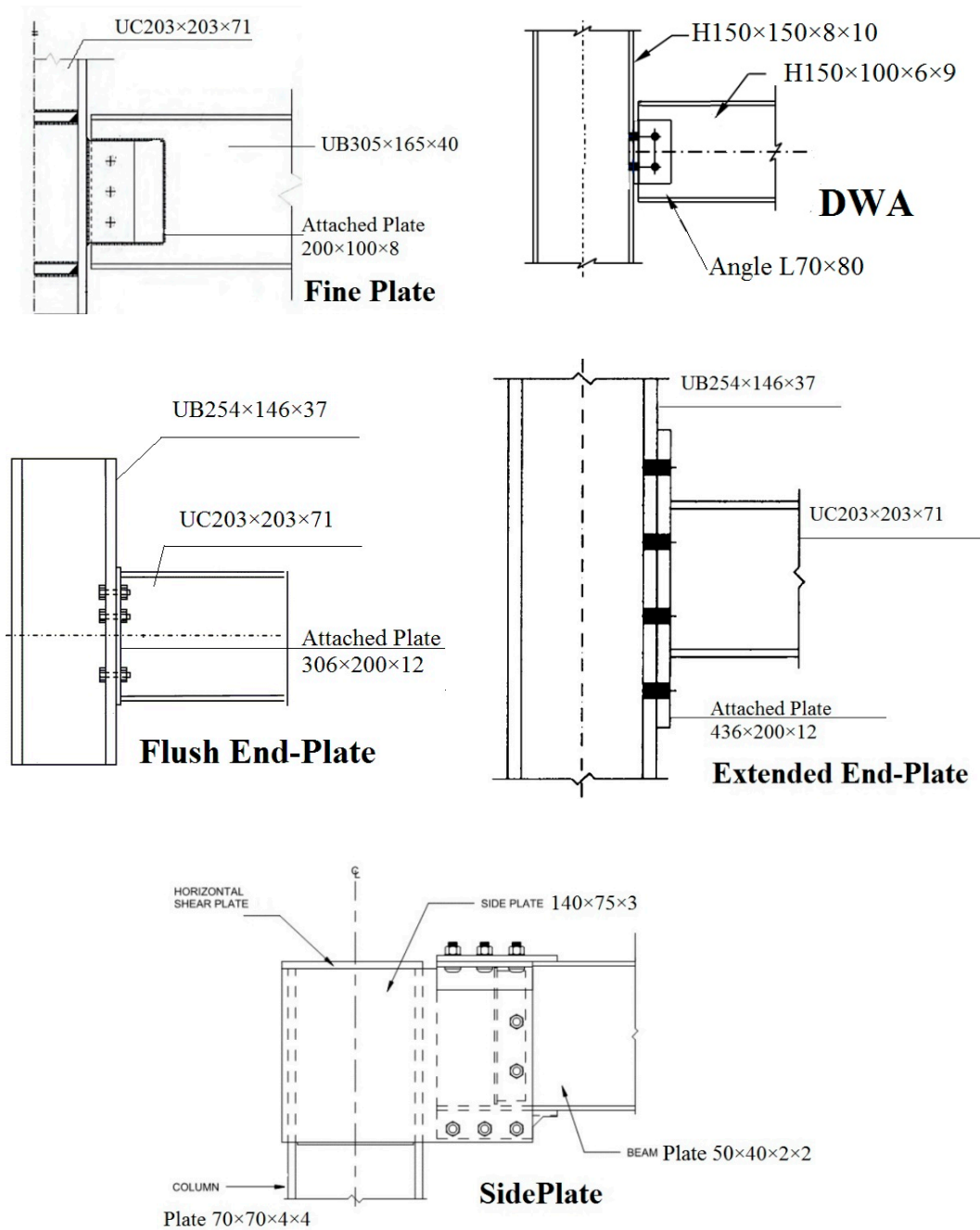
Figure 3. *Cont.*

Figure 3. Configuration and geometric details of studied connections.

Table 2 shows the information of the tested specimens, including the connection type, connection category, and relevant references. In this research, there was an emphasis to select double-span assemblies having similar span-to-depth ratios, R_i. One important implication of this procedure is that it enables an adequate comparison between different types of beam-to-column connections since the effects of different spans and beam sections were filtered out.

Table 2. Summary of Tested Specimens.

Specimen	Connection Type	Connection Category	Span-to-Depth Ratio R_i	Reference
WUF	Welded Unreinforced Flange-Welded Web	Fully rigid	10	W Zhong et al. [41]
SidePlate	SidePlate		20	Faridmehr et al. [42]
I-W	Welded Flange-Weld Web Connection		7.5	W Wang et al. [43]
I-WB	Welded Flange-Bolted Web Connection		7.5	W Wang et al. [43]
ST-WB	Welded Flange-Bolted Web Connection with Shear Diaphragm		7.5	W Wang et al. [43]
DWA	Double Web Angle	Flexible	10	W Zhong et al. [41]
TSWA (L = 8 mm)	Top and Seat-Web Angle		7.9	B Yang et al. [44]
Web Cleat	Web Cleat		7.9	B Yang et al. [44]
Top and Seat angle	Top and Seat Angle		7.9	B Yang et al. [44]
Fine Plate	Fine Plate		7.9	B Yang et al. [44]
TSWA (L = 10 mm)	Top and Seat-Web Angle	Semi-rigid	10	W Zhong et al. [41]
TSWA (L = 12 mm)	Top and Seat-Web Angle		9.5	B Yang et al. [44]
Extended End-Plate	Extended End-Plate		9.5	B Yang et al. [44]
Flush End-Plate	Flush End-Plate		9.5	B Yang et al. [44]

4. Test Results

Table 3 shows the summary of test results, including maximum vertical loads, displacement, connection rotation, and failure mode.

Table 3. Summary of Test Results.

Specimen	$max\frac{F}{F_p}$	$max\frac{\theta}{\theta_p}$	Failure Mode
Fully rigid			
WUF	1.45	11.77	Fracture at the flange
SidePlate	6.38	8.3	Beam failure
I-W	1.25	7.27	Bottom flange and beam web fractured, weld fracture
I-WB	1.25	16	Fracture of shear plate and bottom flange
ST-WB	1.25	15.4	Fracture of shear plate and bottom flange
Semi-rigid			
TSWA (L = 10 mm)	2.24	21.3	Fracture at the angle and failure of the web bolt
TSWA (L = 12 mm)	1.72	17.3	Fracture bolt
Extended end-plate	0.91	14.22	Fracture of weld
Flush end-plate	1.17	12.6	Bolt thread stripping
Flexible			
DWA	1.2	20.4	Fracture at the shear angles
TSWA (L = 8 mm)	0.62	10.9	Fractured web angle
Web Cleat	0.68	10.54	Fractured angle
Top and Seat angle	0.25	16.4	Fractured bottom angle
Fine Plate	0.46	7.6	Bolt fractured in shear

Since the pushdown force is applied to the middle column, the vertical displacement gradually increases. In simple connections such as top and seat angle where the connection possesses a limited capacity to develop the full plastic moment of connected beams, the specimen rotates at both ends following a major deflection below the removed column. The normalized force versus normalized rotation for all tested simple connections is shown in Figure 4. Figure 4 indicates that at the initial pushdown stage, there is no substantial loading resistance. The average F/F_p is around 0.2 at the normalized rotation of 5, until developing axial tensile force in the connected beam as a result of large deflection, indicating the beginning of catenary action. Besides, the shear fracture of bolts causes several jumps in the curve in which the connections experience major localized bearing deformations in the vicinity of bolt holes. Overall, the previous literature indicated that axial tensile force has a major contribution toward progressive collapse resistance in flexible double-span assemblies in which the catenary mechanism takes place before connection component rupture or shear fracture of bolts. Also, the important feature of progressive collapse performance of flexible connections is that although double-span assemblies experienced large deformation, the connected beam remains in the elastic region and connection components experience large plastic strain.
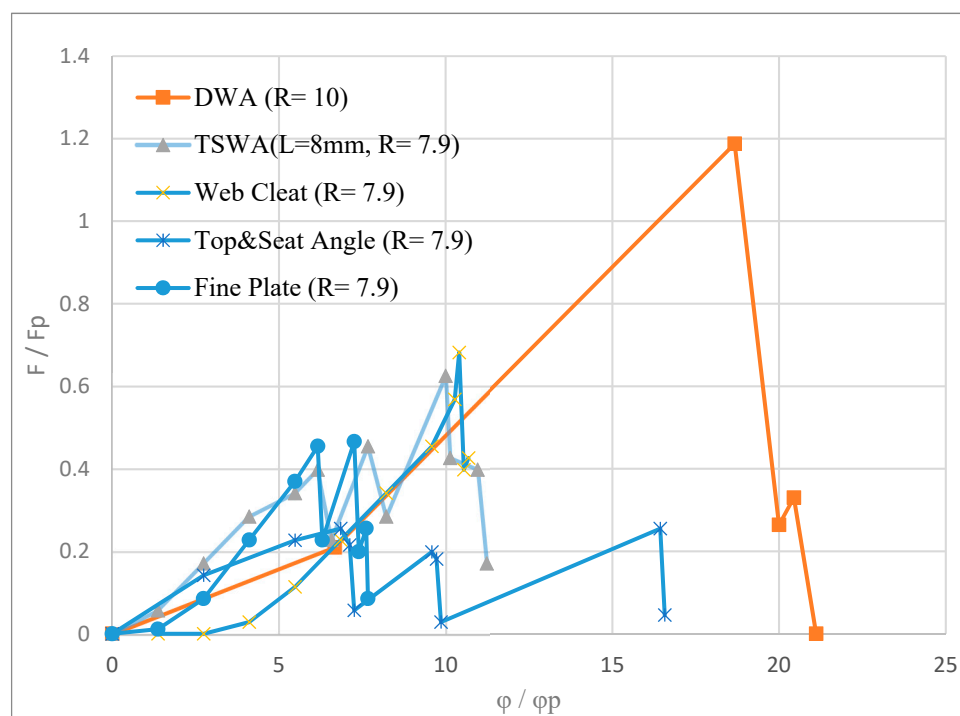

Figure 4. Normalized pushdown resistance against normalized rotation of flexible connections.

The normalized force versus normalized rotation for all tested semi-rigid connections is shown in Figure 5. Figure 5 indicates that semi-rigid connections have higher initial stiffness as a result of high flexural capacity. Nevertheless, after normalized rotation of 5, the stiffness experiences a decrease in most of the specimens as a result of limited capacity connections' components, i.e., top and seat angles. Overall, the previous literature indicates that connections in this category mainly fail due to bolt thread stripping and fracture or fracture at the web angles. Besides, connection failure is categorized in two phases, in which, at the first phase, the connection resists vertical pushdown force through flexural action, and after large plastic rotation, the connections go into the catenary mechanism, indicating phase 2.
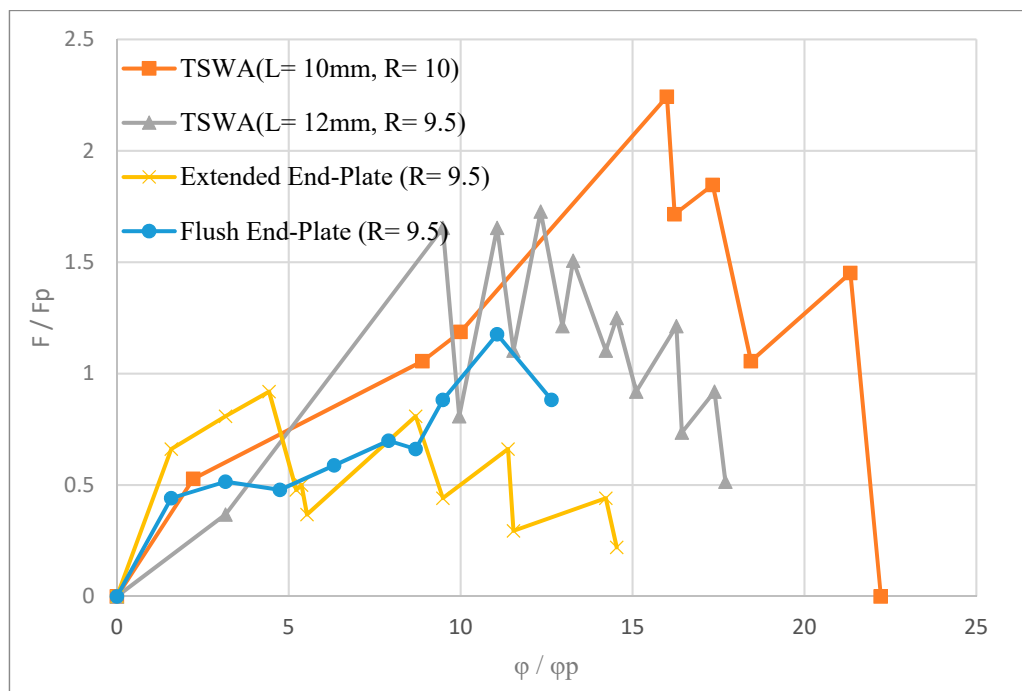
Figure 5. Normalized pushdown resistance against normalized rotation of semi-rigid connections.

The normalized force versus normalized rotation for all tested fully rigid connections is shown in Figure 6. This category possesses the highest stiffness, where in the normalized rotation of around 2, almost all specimens develop the full plastic moment of connected beams. In addition, Figure 6 shows that by considering unique configuration and large R_i, SidePlate has the highest stiffness and ultimate strength. Generally, the previous literature indicated that ductility demand for traditional rigid connections in the case of column removal is mainly controlled by the column shear panel zone, while in the SidePlate connection, it is controlled by a connected beam. Also, in fully rigid connections, the fracture at beam flange or shear plate are the main reasons for failure mode without premature weld or connection's component failure.
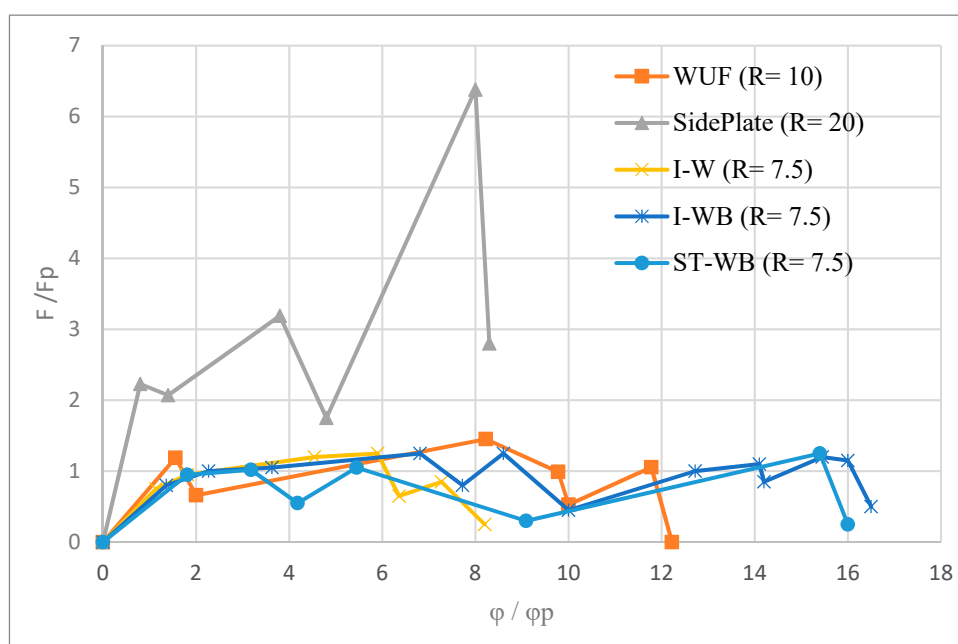

Figure 6. Normalized pushdown resistance against normalized rotation of fully rigid connections.

Yield mechanisms and failure modes are the factors that control both the resistance and ductility or rotational capacity of the connection. Failure modes and yield mechanisms are related but are inherently different. Failure modes cause fracture, loss of deformation capacity, or significant loss of resistance. Yield mechanisms induce inelastic deformation and result in dissipation of energy and changes in stiffness without inducing fracture or excessive loss of resistance. In fully rigid connections, the ratio of rotational capacity of connection to rotational capacity of beam ($\frac{\varphi}{\varphi_p}$) is around 12, where the failure mode is controlled by fracture at shear plate and beam flange. For some specimens in this category, such as I-W, weld fracture causes significantly less ductility, energy dissipation, and plastic rotational capacity. The ratio of $\frac{\varphi}{\varphi_p}$ is around 16 and 13 for semi-rigid and flexible connections, respectively. The failure modes in semi-rigid connections are governed by local buckling and deterioration caused by the large inelastic deformation web cleats and bolts. So, it can be concluded that semi-rigid connections provide large ductility and a ductile failure mode compared to fully rigid connections.

5. Discussions of Test Results

5.1. Catenary Mechanism

A steel beam is mainly subjected to the combined effect of shear force and bending moment under the gravity loading condition, whereas there is no considerable axial force. In the case of sudden column removal, the bending moment at both ends and mid-span of the beam will increase accordingly, resulting in large deflection, developing plastic hinges in these particular locations. In this situation, the beam will experience significant axial force. As the axial force increases gradually, the whole cross-section will experience yielding, resulting in reducing bending moment at plastic hinge locations. At the final stage, the resistance to the external loading only depends on the axial capacity of the beam. This process is generally recognized in the engineering community as tensile catenary action.

The pushdown force versus vertical deflection for a beam with axially restrained support is plotted in Figure 7 [44]. Figure 7a is representative of the behavior of all tested specimens in which failure takes place at a different stage of their response depending on rotation and ductility capacity. In the elastic range, the behavior is generally controlled by connection stiffness, while at the post-elastic stage (beyond point B), the behavior largely depends on geometric and material nonlinearity. Depending on connection categories, different behavior is observed during the different stages, as shown in the typical graph of Figure 7b. Generally, the connected beams and connections are subjected to relatively high axial compression and bending moment at the compressive arching stage, leading to premature instability in the vicinity of compressive components. After point C, the compressive arching impact steadily declines, and the beam axial compression force is converted to tensile (after point D). By increasing the axial tension, the connection's bending moment becomes less significant and they experience severe tensile deformation. Finally, following the point E, the catenary tensile action becomes the governing force-carrying mechanism.

Considering a tensile catenary stage in the beam in the case of sudden column removal (point D onward in Figure 7b), a simplified model for plastic interaction between axial force and bending moment is developed according to the following assumptions:

i.   The beam has an I-shaped section with elastic/perfectly plastic material.
ii.   Plastic hinges only appear at the mid-span and both ends, and hinges follow the rigid-plastic model.
iii. The beam has symmetric restraint with the elastic response.
iv.   The restraint of the steel beam is symmetric and in elastic response.
v.   Once the whole I-section experiences yielding, the correlation between axial force and bending moment controls the behavior of the catenary mechanism.
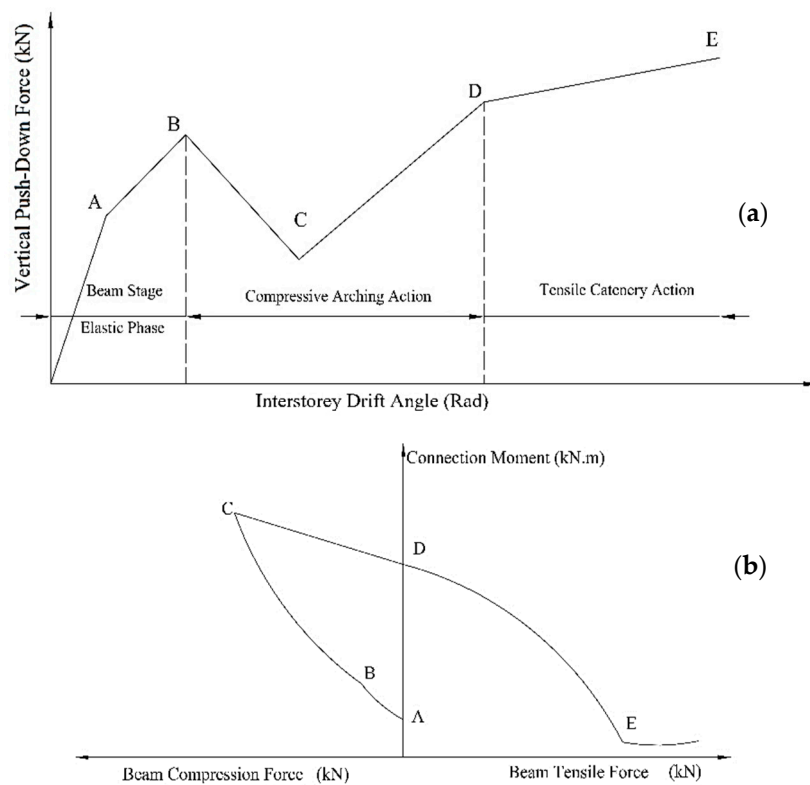
Figure 7. Beam and connection performance following column removal. (**a**) beam nonlinear load-deflection response, (**b**) beam axial load - connection moment interaction

Assuming the entire cross-section yield, the bending moment and tensile force correlation is given by the following equation in the case where the neutral axis is in the web:

$$\frac{M}{M_y} + \frac{(1+\alpha)^2}{\alpha[2(1+\beta)+\alpha]}\left(\frac{p}{p_y}\right)^2 = 1 \tag{5}$$

where M_y and p_y are the plastic moment capacity and ultimate plastic axial force of the beam respectively, calculated by:

$$M_y = Z f_{ye} \quad p_y = (2A_f + A_w) f_{ye}$$

where f_{ye} is the expected material yield strength, Z is the plastic section modulus, A_f is the beam's flange area, and A_w is the beam's web plate area. β is the ratio of flange thickness to web height, and α is also defined by the following equation:

$$\alpha = A_w/(2A_f)$$

In the case that the plastic neutral axis appears in the beam's flange, the moment and tensile correlation is given by the following equation:

$$\frac{1-\gamma}{1 - \frac{(1+\alpha)^2\gamma^2}{\alpha[2(1+\beta)+\alpha]}} \frac{M}{M_y} + \frac{P}{P_y} = 1 \tag{6}$$

where

$$\gamma = A_w/(2A_f + A_w)$$

Since the web height is much bigger than flange thickness, it is acceptable to assume $\beta = 0$. Accordingly, Equations (5) and (6) can be rewritten as:

$$\frac{M}{M_y} + \zeta \left(\frac{p}{p_y}\right)^2 = 1 \tag{7}$$

$$\lambda \frac{M}{M_y} + \frac{P}{P_y} = 1 \tag{8}$$

where

$$\zeta = \frac{(1+\alpha)^2}{[\alpha(2+\alpha)]}; \; \lambda = \frac{1-\gamma}{1-\zeta\gamma^2}$$

Figure 8a presents the interaction of Equations (7) and (8), indicating that the curves of Equations (7) and (8) intersect at point $\left(1 - \zeta\gamma^2.\gamma\right)$. For simplicity, the nonlinear domain of Equation (7) can be replaced by a straight line, using the following equation:

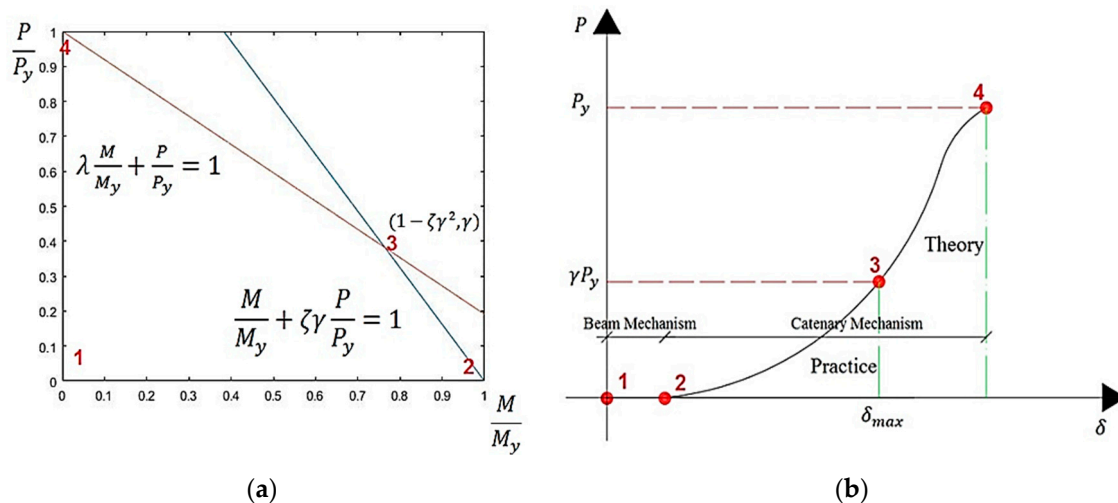$$\frac{M}{M_y} + \zeta\gamma \frac{P}{P_y} = 1 \tag{9}$$

(**a**)   (**b**)

Figure 8. (**a**) Plastic interaction between bending moment and tensile force, and (**b**) beam axial force versus mid-span deflection.

Figure 8b shows the correlation between the beam's axial force and vertical displacement in the case of middle column removal. According to the experimental results, two main different failure mechanisms in the beam are recognized, as presented in Figure 8b. These two failure mechanisms are introduced as the beam mechanism (phase 1 to phase 2) and the catenary mechanism (phase 2 to phase 4), respectively. Experimental results indicate that the tensile force in the beam is smaller than the ultimate plastic axial force before the failure. Accordingly, it is reasonable to assume that the moment of the beam is equal to $1 - \zeta\gamma^2\ M_y$ and the axial force is equal to $\gamma\ P_y$ before the beam experiences failure (refer to practice failure point 3 in Figure 8b).

Figure 9 shows the vertical reaction, V_R, of connection, which can be calculated by Equation (10).

$$V_R = V_i \cos\varphi_i + P_i \sin\varphi_i = F_f + F_c \tag{10}$$

where φ_i, V_i, and P_i are rotation of deflected beam, transverse shear, and axial force in the case of middle column removal, respectively. The internal transverse shear and axial force are measured

through installed strain gauges distributed on a connected beam. F_f in Equation (10) represents flexural mechanism resistance while F_c is the resistance component due to the catenary mechanism.
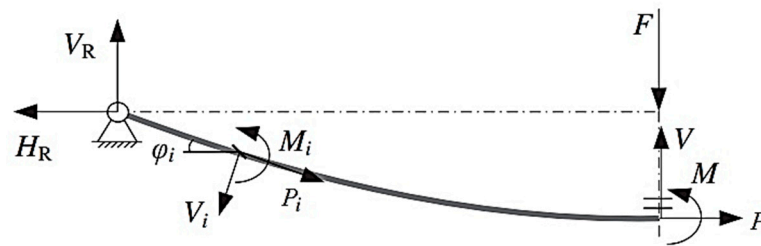

Figure 9. Development of internal forces in the beam-to-column assembly in the case of middle column removal.

Figure 10 shows the development of axial force and bending moment in the case of middle column removal for three tested specimens in reference [43]. According to Figure 10a, at the preliminary phases, the behavior of the beam is controlled by flexural resistance, and the tensile force is almost zero. With increased downward displacement, the axial tension also increases in the beams, developing catenary mechanism until the beam or connection can no longer bear the combined flexural stresses and tensile force and fails (see Figure 10b).
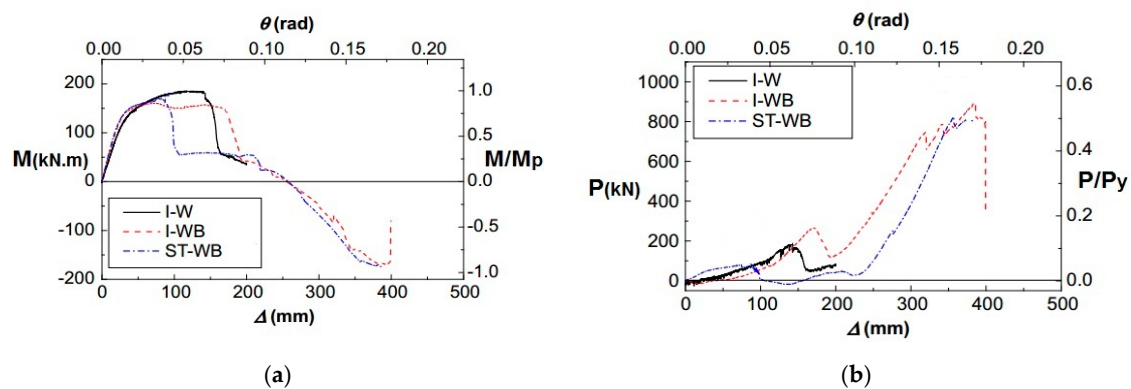

(**a**) (**b**)

Figure 10. Load resistance mechanism: (**a**) development of a flexural mechanism F_f, and (**b**) development of a catenary mechanism F_c.

Figure 10 also indicates that fully rigid connections, I-WB and ST-WB, can develop relatively high axial force and a bending moment of connected beam compared to the I-W specimen. In other words, the type of beam-to-column connection plays an important role in developing the catenary mechanism. This issue is also acknowledged in Figure 11, where the flexible connections, i.e., top and seat angle and TSWA = 8 mm, fail to develop the catenary mechanism of the connected beam. This issue confirms the fact that the failure is mainly concentrated at the connection components in a flexible and semi-rigid connection, and therefore, these types of connections have limited capacity to develop the catenary mechanism.

5.2. Maximum Rotation and Ductility Capacity

In steel structures subjected to sudden column removal, the maximum deformation and rotation capacities of connections within the affected areas have a major contribution to the ultimate load-carrying capacities of the system. The main progressive collapse guidelines, i.e., the Unified Facilities Criteria (UFC) 4 023 03 [45], specify a series of plastic rotation angles for several beam-to-column connection categories based on a nonlinear modeling simulation, as shown in Table 4.
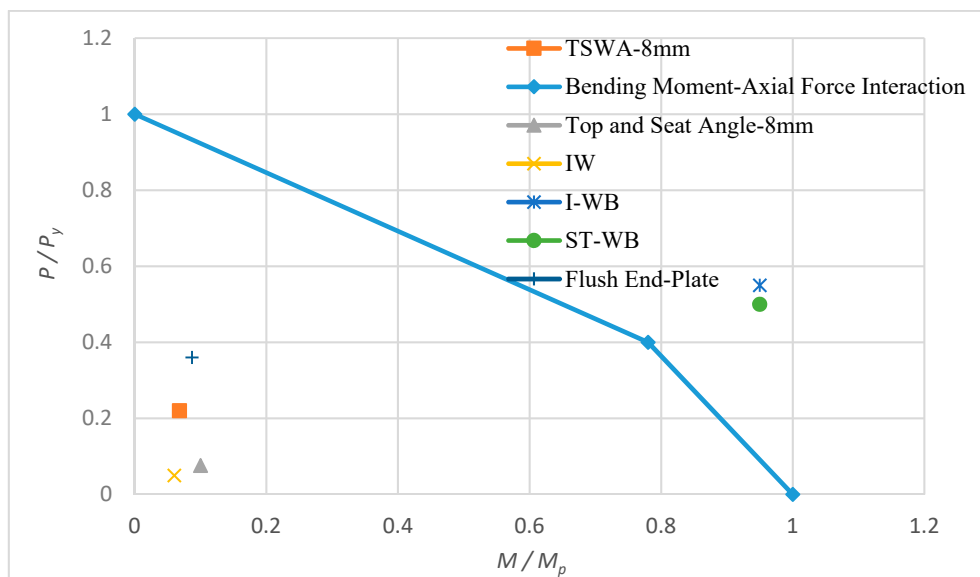
Figure 11. Correlation between axial force and bending moment in studied specimens at the final stage of the pushdown test.

Table 4. Modeling Parameters and Acceptance Criteria for Nonlinear Modeling of Steel Frame Connections.

Connection Type	Nonlinear Modeling Parameters			Nonlinear Acceptance Criteria
	Plastic Rotation Angle (Rad)		Residual Strength Ratio	Plastic Rotation Angle (Rad)
	a	*b*	*c*	Primary Component
Fully Restrained Moment Connections				
WUF	$0.0284 - 0.0004d$	$0.043 - 0.0006d$	0.2	$0.0284 - 0.0004d$
SidePlate®	$0.089 - 0.0005d$	$0.169 - 0.0001d$	0.6	$0.089 - 0.0005d$
Partially Restrained Moment Connections (Relatively Stiff)				
Shear in Bolt	0.036	0.048	0.2	0.03
Tension in Bolt	0.016	0.024	0.8	0.013
Tension in Tee	0.012	0.018	0.8	0.010
Flexure in Tee	0.042	0.084	0.2	0.035
Partially Restrained Simple Connections (Flexible)				
Flexure in Angles	$0.1125 - 0.0027d_{bg}$	$0.150 - 0.0036d_{bg}$	0.4	$0.112 - 0.0027d_{bg}$
Simple Shear Tab	$0.0502 - 0.0015d_{bg}$	$0.072 - 0.0022d_{bg}$	0.2	$0.0502 - 0.0015d_{bg}$

d_{bg} = depth of bolt group, inch; d = depth of beam, inch.

Figure 12 shows the nonlinear force–vertical displacement curve of several fully rigid tested specimens along with idealized multi-linear curves. For a welded unreinforced flange WUF connection, represented by I-WB and ST-WB in this research, the results indicate large ductility when subjected to mid-column removal. The plastic rotation angle *b* for I-WB and ST-WB is around 0.16 rad, well beyond the recommended acceptance criteria by the UFC presented in Table 4. This indicates that tested specimens can resist large plastic rotation without a significant decline in resisting vertical force.
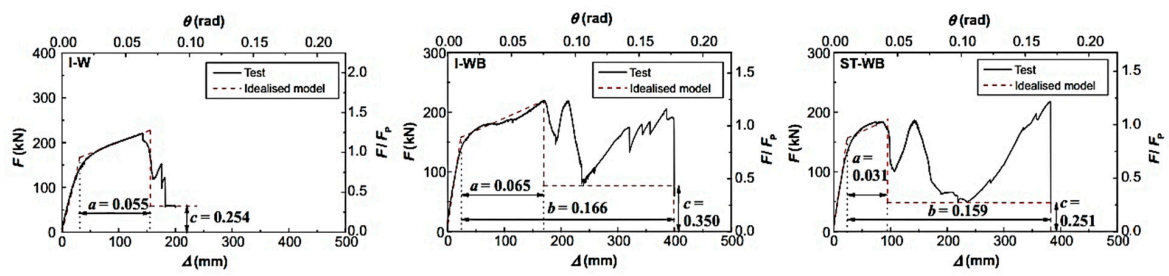
Figure 12. Ductility assessment of fully rigid tested specimens.

In this section, the plastic rotation angle of all tested specimens is compared to the acceptance criteria, estimated based on the depth of the connection, recommended by the UFC. Figures 13–15 show the maximum rotational capacity of studied connections versus connection depth along with the acceptance criteria line recommended by the UFC, as presented in Table 4.
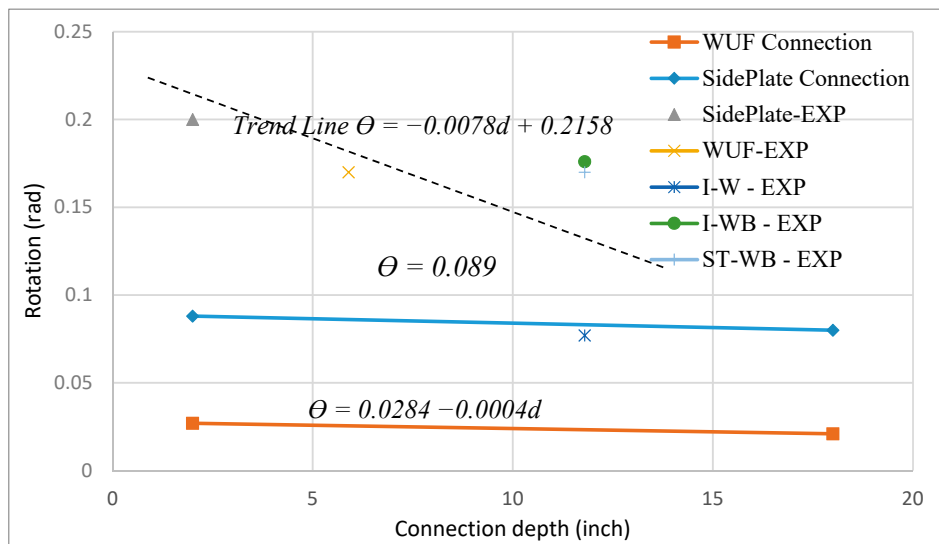

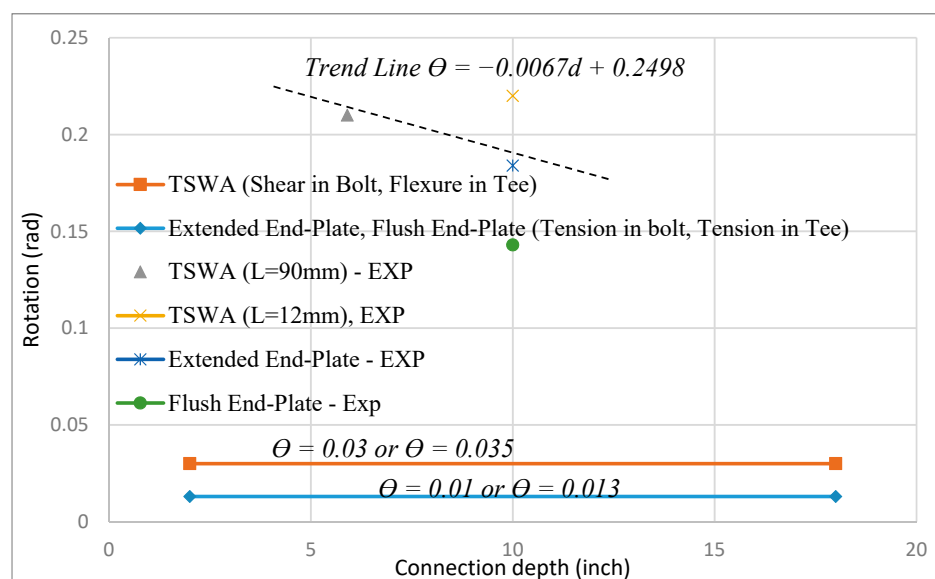**Figure 13.** Maximum rotation capacities versus connection depth for fully rigid connections.

Figure 14. Maximum rotation capacities versus connection depth for semi-rigid connections.
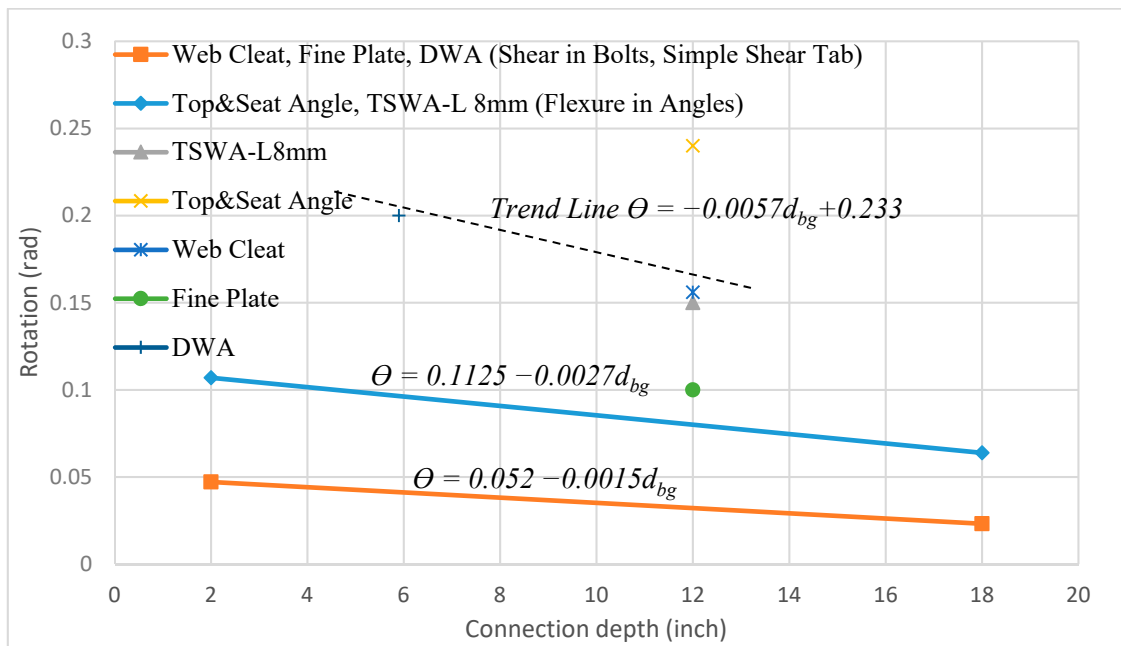
Figure 15. Maximum rotation capacities versus connection depth for flexible connections.

Overall, Figures 13–15 indicate that the average plastic rotation angle varies from 0.1 to 0.2 rad, which significantly surpasses the UFC recommended acceptance criterion. This indicates that all three beam-to-column connection categories can address adequate plastic rotation during sudden column removal. In addition, the results reveal that the suggested ductility acceptance criteria are on the conservative side for all three beam-to-column connection categories. The current in-practice acceptance criteria employed in progressive collapse analysis are based on cyclic simulations proposed by the American Society of Civil Engineers (ASCE/SEI) 41 13 [46] that do not consider large axial demands imposed over sudden column removal. Actually, the results show that the connection depth alone is not a reliable indicator to predict the rotational capacity of a connection, where different connection types with the same R_i result in totally different maximum rotation capacity. Moreover, the results show that although the stiffness of fully rigid connections is higher than flexible connections, both categories result in almost the same rotation capacity, by around 0.15 rad.

The previous literature indicates that the rotational ductility of connections is significantly affected by bolt rupture and brittle failure of welding [47]. In other words, a variation in failure mode will affect the maximum rotational ductility of connections. To meet the criterion for rotation capacity, in this research, an acceptance criterion is proposed by considering initial stiffness and the design flexural resistance. To this end, the maximum rotation capacity of the connection, φ_u, is defined by the rotation at the point where either (i) the connection resistance has dropped to 0.8 M_n, or (ii) the deformation is more than 0.03 rad. The first yielding rotation φ_y is also defined as follows:

$$\varphi_y = \frac{\frac{2}{3} M_y}{S_{j.ini}} \tag{11}$$

The above-mentioned parameters have been used to determine the ductility of studied connections. The ability to sustain large inelastic deformations without significant loss in strength is referred to as ductility, μ, and is defined as follows:

$$\mu = \frac{\varphi_u}{\varphi_y} \tag{12}$$

Figure 16 illustrates the nonlinear idealization of the moment-rotation curve of a typical steel beam-to-column connection.
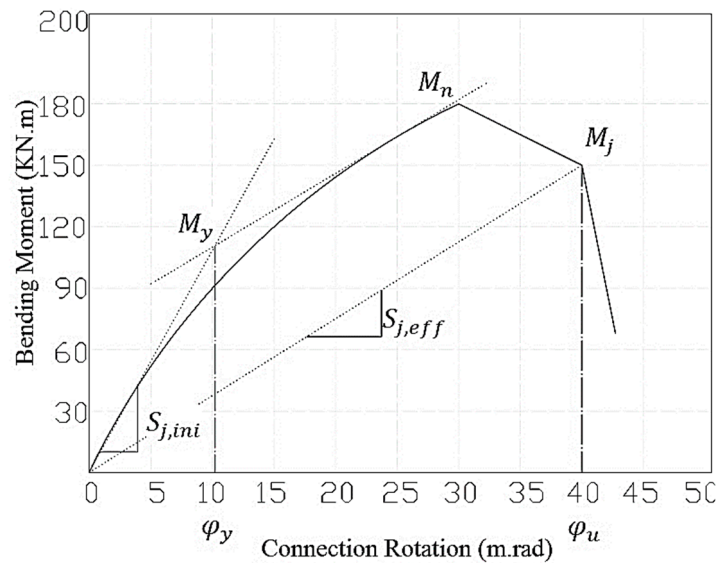
Figure 16. Typical moment-rotation response.

Table 5 illustrates the yielding rotation, maximum rotation capacity, and ductility of studied specimens. Table 5 indicates that fully rigid and semi-rigid connections result in bigger ductility compared to flexible connections. Generally, in a situation where the connection strength exceeds the beam strength, the ductility of the whole system is controlled by the beam, and the connection remains elastic. For instance, the behavior and overall ductility of the SidePlate moment connection system are defined by the plastic rotational capacity of the beam, where the limit state is ultimately the failure of the beam flange, away from the connection. On the other hand, if the beam capacity exceeds the connection capacity, then deformations only take place in the connection itself.

Table 5. Yielding Rotation, Maximum Rotation Capacity, and Ductility of Studied Specimens.

Specimen	φ_y (rad)	φ_u (rad)	μ
WUF	0.023	0.176	7.6
SidePlate	0.02	0.19	9.5
I-W	0.018	0.067	3.7
I-WB	0.02	0.168	8.4
ST-WB	0.019	0.17	8.9
TSWA (L = 10 mm)	0.033	0.32	9.6
TSWA (L = 12 mm)	0.025	0.23	9.2
Extended end-plate	0.02	0.184	8.9
Flush end-plate	0.02	0.143	7.1
DWA	0.065	0.36	5.53
TSWA (L = 8 mm)	0.061	0.149	2.44
Web Cleat	0.041	0.156	3.8
Top and Seat angle	0.041	0.246	6
Fine Plate	0.03	0.108	3.6
Average			6.73

5.3. Stiffness Degradation

Steel beam-to-column connections will experience stiffness degradation when subjected to cyclic loading. It has conclusively been shown that the stiffness will decrease by increasing the inter-storey drift angle in steel beam-to-column connections [48]. Meanwhile, there is reliable evidence that the metal material behaves differently when subjected to monotonic and impact loading [49]. However, far too little attention has been paid to stiffness degradation of steel material under strong impact loading. Since the available data solely consider the monotonic loading for simulating sudden column

removal, in this study, initial stiffness, $S_{j.ini}$, and secant stiffness, $S_{j.eff}$, were taken into account to evaluate the stiffness degradation. Secant or effective stiffness, $S_{j.eff}$, is defined as the ratio of bending moment before substantial loss of strength to the maximum rotation φ_u, as shown in Figure 16.

$$S_{j.eff} = \frac{M_j}{\varphi_u} \tag{13}$$

Table 6 shows the normalized initial and secant stiffness as well as the connected beam stiffness for all studied specimens before substantial strength degradation. The initial and secant stiffness are normalized with respect to the connected beam stiffness. Table 6 clearly indicates that fully rigid specimens, i.e., SidePlate and I-WB, possess much higher stiffness compared to semi-rigid and flexible specimens. It is also evident that although the initial stiffness in flexible connections is negligible, they can maintain the stiffness where the secant stiffness is almost three times higher than the initial stiffness (consider the web cleat and fine plate specimens).

Table 6. Stiffness Properties of the Studied Specimens.

Specimen	$\frac{EI_b}{L_b}$ ($\frac{KN \cdot m}{rad}$)	Normalized $S_{j.ini}$	Normalized $S_{j.eff}$
WUF	1295.3	3.02	0.35
SidePlate	20.2	17.3	4.95
I-W	5457.6	1.37	0.36
I-WB	5457.6	2.02	0.19
ST-WB	5457.6	2.55	0.24
TSWA (L = 10 mm)	1295.3	0.93	0.26
TSWA (L = 12 mm)	4420	0.35	0.16
Extended end-plate	4420	1.08	0.09
Flush end-plate	4420	0.79	0.27
DWA	1295.3	0.12	0.06
TSWA (L = 8 mm)	6787.7	0.07	0.06
Web Cleat	6787.7	0.019	0.06
Top and Seat angle	6787.7	0.09	0.02
Fine Plate	6787.7	0.014	0.06

The normalized stiffness degradation versus inter-storey drift angle plots for all specimens are shown in Figures 17–19. Figure 17 generally indicates that by increasing inter-storey drift angles, the normalized stiffness decreases, although the SidePlate connection has considerably higher initial stiffness as well as lower degradation slope. This stiffer behavior is attributed to the distribution of the hinge formation mechanism due to the presence of two side plates wrapping around the shear panel joint region, resulting in increased stiffness of the subassembly. Generally, in this category, flexural action controls the stiffness of the specimens in the early stage of the response.

Figure 18 shows that semi-rigid connections have an irregular pattern for stiffness degradation, where elementary step stiffness experiences degradation, whereas at higher inter-storey drift angle, the stiffness remains constant or even increases before the failure of the specimen. This irregular pattern can be explained by desirable features of extremely high ductility (rotational capacity) and developing catenary action.

Figure 19 indicates that although the flexible connections have considerably lower stiffness compared to fully rigid and flexible connections, they can develop the initial stiffness as the inter-storey drift angle increases. On average, the initial stiffness increases up to 100 percent when the inter-storey drift angles reach around 0.1 rad. This behavior can be explained by the connection geometry that allows rotation at preliminary steps, whereas the tensile capacity of connections' components, i.e., web cleat, bolts, etc., along with stiffness hardening at higher drift angles, resists against rotation and subsequently develops the stiffness.
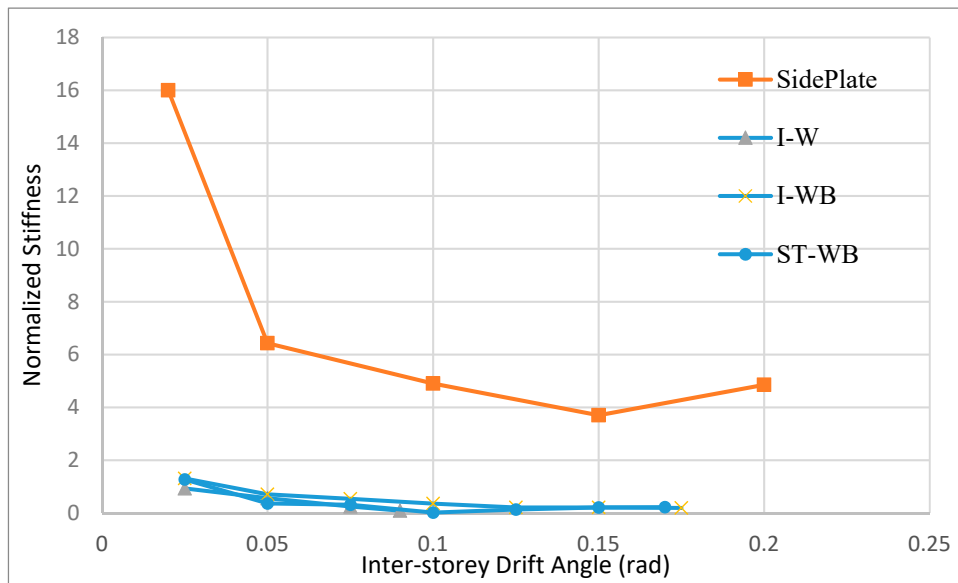
Figure 17. Stiffness degradation versus inter-storey drift angle for fully rigid connections.
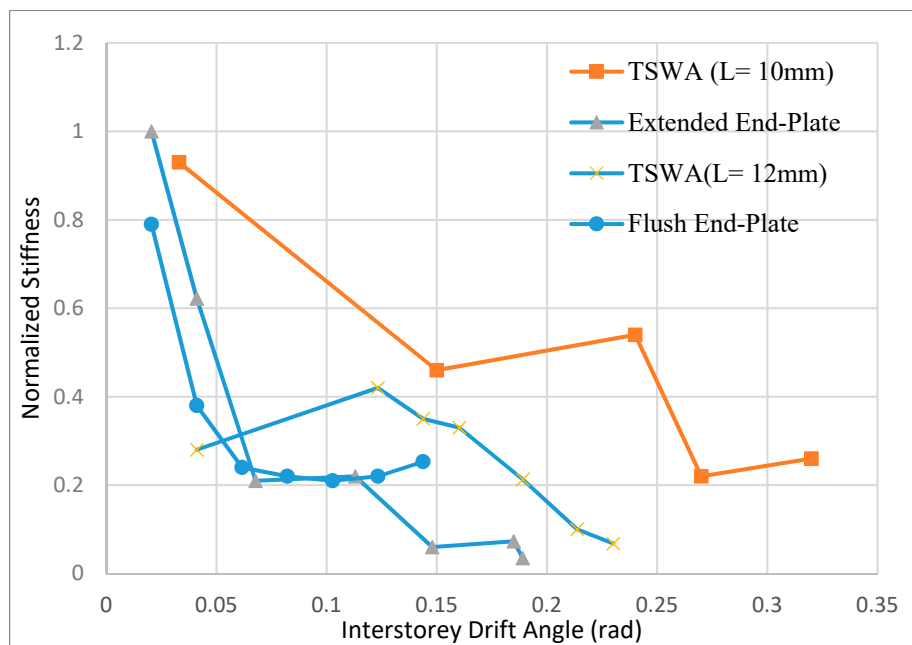

Figure 18. Stiffness degradation versus inter-storey drift angle for semi-rigid connections.

Stiffness degradation is an important aspect of seismic design since a large deformation leads to P-Delta effects, eventually destabilizing the structure. Several codes and regulations prescribe recommendations for stiffness and strength degradation as a measure in seismic design. For instance, the AISC seismic provisions recommend that the connection must sustain an inter-storey drift angle of at least 0.04 rad, while the flexural resistance at the column face must be equal to at least 0.80 M_p of the connected beam. Overall, according to the results of this study, it is recommended that the stiffness at an inter-storey drift angle of 0.05 rad should be larger than 75% of the initial stiffness to develop a reliable catenary mechanism.
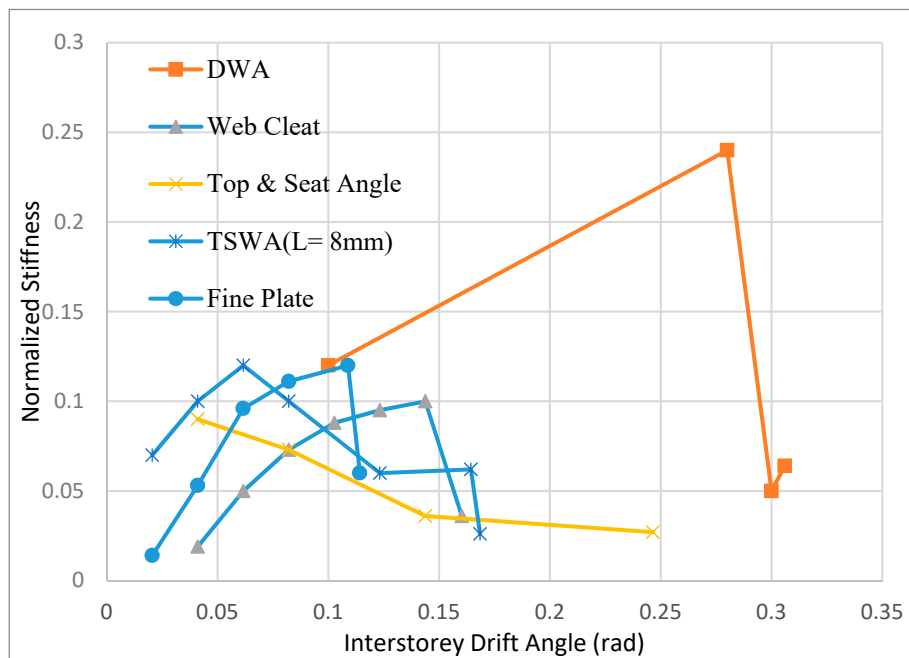
Figure 19. Stiffness degradation versus inter-storey drift angle for flexible connections.

5.4. Evaluation of Catenary and Flexural Mechanisms Under Different R_i

This section investigates the influence of different R_i on flexural and catenary mechanisms. As discussed in Section 5.1, under the middle column removal condition, the vertical resistance of the beam-to-column connection is controlled by the contribution of flexural and catenary mechanisms. Figure 19 illustrates the gravity resistance development for the beam-column assembly of two specimens, having welded unreinforced flange-bolted web (WUF-BW) connections with the same beam section but different R_i, as investigated by Li et al. [25]. The flexural (f_f) and the catenary (f_c) mechanisms, recognized as two components of the gravity resistance, are separately plotted in Figure 20a respectively, and subsequently, their resultant is plotted in Figure 20b. Three distinctive phases are recognized, as shown in the line graphs, introduced by the flexure action-dominated phase I, the combination of flexure-catenary mechanism phase II, and finally, the catenary-dominated mechanism phase III. These three phases are normally separated from each other by the formation of a plastic hinge followed by an initial fracture in the connection's components.
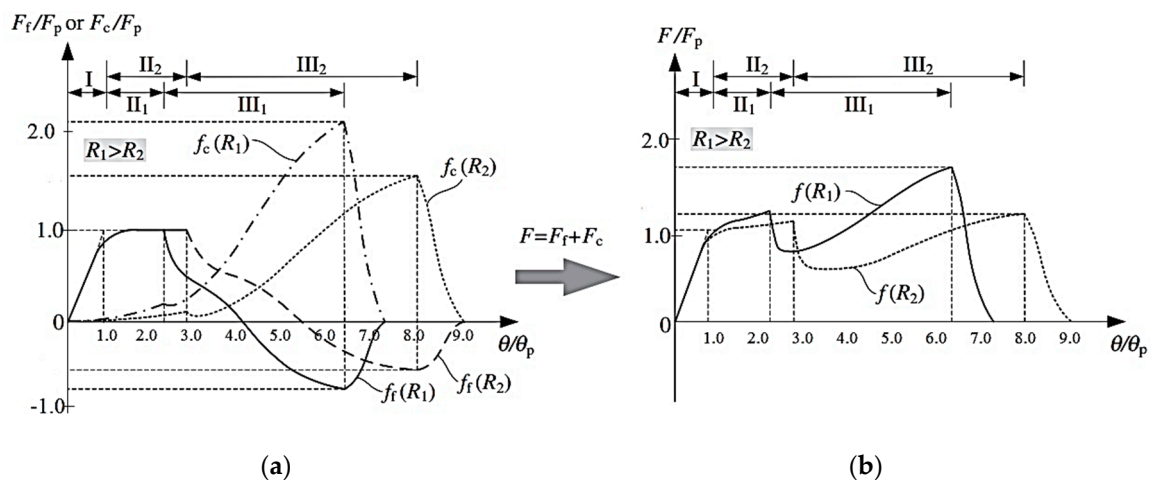

(a)   (b)

Figure 20. Gravity resistance development for beam-to-column assembly: (**a**) flexural and catenary mechanism, and (**b**) overall gravity resistance.

It is evident that a specimen with larger R_i (R_1) can provide a higher vertical resistance as a result of higher catenary mechanism response. However, the specimen with lower R_i (R_2) results in a larger chord rotation ratio, leading to a more ductile response.

6. Summary and Conclusions

This paper presented the descriptions and experimental results of available full-scale double-span systems subjected to the middle column loss scenario. Several parameters and features including beam span-to-depth ratio, catenary mechanism, stiffness, and ductility have been investigated for fully rigid, semi-rigid, and flexible connections. The following conclusions can be drawn:

I. After middle column removal at the preliminary phases, the behavior of the beam is controlled by flexural resistance, and the tensile force is almost zero, recognized as a flexure action-dominated phase. With increased downward displacement, the axial tension also increases in the beams, developing a catenary mechanism recognized as a catenary-dominated mechanism phase. The results of this research show that the magnitude of axial force in the flexible connections, i.e., top and seat angle, is significantly small compared to fully rigid connections. This phenomenon can be justified by the failure mechanism that develops in the connection's components rather than the connected beam, preventing the catenary mechanism development.

II. The maximum rotation capacity versus connection depth for almost all beam-to-column connection categories significantly surpasses the DoD's recommended acceptance criterion. The suggested acceptance criteria are on the conservative side as it only considers pure flexural resistance. Therefore, connection depth alone is not a reliable indicator to predict the rotational capacity of beam-to-column connections.

III. The stiffness in fully rigid and semi-rigid connections generally experiences a decrease by increasing inter-storey drift angle. On the other hand, the flexible connections have a potential to develop the initial stiffness as the inter-storey drift angle increases. Such behavior can be explained by the geometry of these types of connections that allows rotation at preliminary steps, while the stiffness can be developed at higher drift angles depending on tensile capacity of connections' components and stiffness hardening.

Author Contributions: Original draft preparation, numerical models, validation, and methodology: I.F.; supervision, review, and editing: M.H.B. All authors have read and agreed to the published version of the manuscript.

Conflicts of Interest: The authors declare no conflict of interest.

References

1. Pantidis, P.; Cao, L.; Gerasimidis, S. Partial Damage Distribution and Progressive Collapse of Buildings. In *Structures Congress 2020*; American Society of Civil Engineers: Reston, VA, USA, 2020.
2. Brunesi, E.; Nascimbene, R.; Parisi, F.; Augenti, N. Progressive collapse fragility of reinforced concrete framed structures through incremental dynamic analysis. *Eng. Struct.* **2015**, *104*, 65–79. [CrossRef]
3. Masoero, E.; Wittel, F.K.; Herrmann, H.J.; Chiaia, B.M. Progressive collapse mechanisms of brittle and ductile framed structures. *J. Eng. Mech.* **2010**, *136*, 987–995. [CrossRef]
4. Agarwal, A.; Varma, A.H. Fire induced progressive collapse of steel building structures: The role of interior gravity columns. *Eng. Struct.* **2014**, *58*, 129–140. [CrossRef]
5. Kim, J.; Park, J. Design of steel moment frames considering progressive collapse. *Steel Compos. Struct.* **2008**, *8*, 85–98. [CrossRef]
6. Cassiano1a, D.; D'Aniello, M.; Rebelo, C.; Landolfo, R.; da Silva, L.S. Influence of seismic design rules on the robustness of steel moment resisting frames. *Steel Compos. Struct.* **2016**, *21*, 479–500. [CrossRef]
7. Zhu, F.Y.; Chen, C.H.; Yao, Y.; Keer, L.M.; Huang, Y. Dynamic increase factor for progressive collapse analysis of semi-rigid steel frames. *Steel Compos. Struct.* **2018**, *28*, 209–221.

8.   Byfield, M.; Mudalige, W.; Morison, C.; Stoddart, E. A review of progressive collapse research and regulations. *Proc. ICE Struct. Build.* **2014**, *167*, 447–456. [CrossRef]

9.   Gsa, U. *Progressive Collapse Analysis and Design Guidelines for New Federaloffice Buildings and Major Modernization Projects*; The US General ServicesAdministration: Washington, DC, USA, 2003.

10.   Department of Defense. *Design of Buildings to Resist Progressive Collapse*; Unified Facilities Criteria (UFC)-DoD. 2005. Available online: https://www.wbdg.org/FFC/DOD/UFC/ARCHIVES/ufc_4_023_03_2009_c2.pdf (accessed on 18 July 2020).

11.   Wang, F.; Yang, J.; Pan, Z. Progressive collapse behaviour of steel framed substructures with various beam-column connections. *Eng. Fail. Anal.* **2020**, *109*, 104399. [CrossRef]

12.   Wang, H.; Tan, K.H.; Yang, B. Experimental Tests of Steel Frames with Different Beam–Column Connections under Falling Debris Impact. *J. Struct. Eng.* **2020**, *146*, 04019183. [CrossRef]

13.   Alrubaidi, M.; Elsanadedy, H.; Abbas, H.; Almusallam, T.; Al-Salloum, Y. Investigation of different steel intermediate moment frame connections under column-loss scenario. *Thin Walled Struct.* **2020**, *154*, 106875. [CrossRef]

14.   Guo, L.; Gao, S.; Fu, F. Structural performance of semi-rigid composite frame under column loss. *Eng. Struct.* **2015**, *95*, 112–126. [CrossRef]

15.   Zhang, J.; Jiang, J.; Xu, S.; Wang, Z. An investigation of the effect of semi-rigid connections on sudden column removal in steel frames. In *Structures*; Elsevier: Amsterdam, The Netherlands, 2018.

16.   Xu, G.; Ellingwood, B.R. Disproportionate collapse performance of partially restrained steel frames with bolted T-stub connections. *Eng. Struct.* **2011**, *33*, 32–43. [CrossRef]

17.   Dinu, F.; Marginean, I.; Dubina, D. Experimental testing and numerical modelling of steel moment-frame connections under column loss. *Eng. Struct.* **2017**, *151*, 861–878. [CrossRef]

18.   Zahrai, S.M.; Ezoddin, A. Cap truss and steel strut to resist progressive collapse in RC frame structures. *Steel Compos. Struct.* **2018**, *26*, 635–647.

19.   Liu, C.; Tan, K.H.; Fung, T.C. Component-based steel beam–column connections modelling for dynamic progressive collapse analysis. *J. Constr. Steel Res.* **2015**, *107*, 24–36. [CrossRef]

20.   Tay, C.G.; Koh, C.G.; Liew, J. Efficient progressive collapse analysis for robustness evaluation of buildings experiencing column removal. *J. Constr. Steel Res.* **2016**, *122*, 395–408. [CrossRef]

21.   Qin, X.; Wang, W.; Chen, Y.; Bao, Y. Experimental study of through diaphragm connection types under a column removal scenario. *J. Constr. Steel Res.* **2015**, *112*, 293–304. [CrossRef]

22.   Faridmehr, I.; Osman, M.H.; Nejad, A.F.; Tahir, M.M.; Azimi, M. Seismic and Progressive Collapse Assessment of New Proposed Steel Connection. *Adv. Struct. Eng.* **2015**, *18*, 439–452. [CrossRef]

23.   Li, L.; Wang, W.; Chen, Y.; Teh, L.H. A basis for comparing progressive collapse resistance of moment frames and connections. *J. Constr. Steel Res.* **2017**, *139*, 1–5. [CrossRef]

24.   Stylianidis, P.; Nethercot, D.; Izzuddin, B.; Elghazouli, A.Y. Study of the mechanics of progressive collapse with simplified beam models. *Eng. Struct.* **2016**, *117*, 287–304. [CrossRef]

25.   Li, L.; Wang, W.; Teh, L.H.; Chen, Y. Effects of span-to-depth ratios on moment connection damage evolution under catenary action. *J. Constr. Steel Res.* **2017**, *139*, 18–29. [CrossRef]

26.   Rezvani, F.H.; Yousefi, A.M.; Ronagh, H.R. Effect of span length on progressive collapse behaviour of steel moment resisting frames. In *Structures*; Elsevier: Amsterdam, The Netherlands, 2015.

27.   Sun, R.R.; Burgess, I.W.; Huang, Z.; Dong, G. Progressive failure modelling and ductility demand of steel beam-to-column connections in fire. *Eng. Struct.* **2015**, *89*, 66–78. [CrossRef]

28.   Kuhlmann, U.; Rölle, L.; Izzuddin, B.A.; Pereira, M.F. Resistance and Response of Steel and Steel–Concrete Composite Structures in Progressive Collapse Assessment. *Struct. Eng. Int.* **2012**, *22*, 86–92. [CrossRef]

29.   Liu, Y.; Málaga-Chuquitaype, C.; Elghazouli, A.Y. Behaviour of open beam-to-tubular column angle connections under combined loading conditions. *Steel Compos. Struct.* **2014**, *16*, 157–185. [CrossRef]

30.   Goldaran, R.; Turer, A. Application of acoustic emission for damage classification and assessment of corrosion in pre-stressed concrete pipes. *Measurement* **2020**, *160*, 107855. [CrossRef]

31.   Hadidi, A.; Jasour, R.; Rafiee, A. On the progressive collapse resistant optimal seismic design of steel frames. *Struct. Eng. Mech.* **2016**, *60*, 761–779. [CrossRef]

32.   Kordbagh, B.; Mohammadi, M. Influence of seismicity level and height of the building on progressive collapse resistance of steel frames. *Struct. Des. Tall Spec. Build.* **2017**, *26*, e1305. [CrossRef]

33. Chen, J.; Shu, W.; Huang, H. Rate-Dependent Progressive Collapse Resistance of Beam-to-Column Connections with Different Seismic Details. *J. Perform. Constr. Facil.* **2017**, *31*, 04016086. [CrossRef]

34. Yang, B.; Tan, K.H. Robustness of Bolted-Angle Connections against Progressive Collapse: Experimental Tests of Beam-Column Joints and Development of Component-Based Models. *J. Struct. Eng.* **2013**, *139*, 1498–1514. [CrossRef]

35. Jamshidi, A.; Koduru, S.; Driver, R.G. Reliability Analysis of Shear Tab Connections under Progressive Collapse Scenario. In *Structures Congress 2014*; ASCE: Reston, VA, USA, 2014.

36. Qin, C.B.; Chian, S.C.; Yang, X.L. 3D Limit Analysis of Progressive Collapse in Partly Weathered Hoek–Brown Rock Banks. *Int. J. Geomech.* **2017**, *17*, 04017011. [CrossRef]

37. Oosterhof, S.A.; Driver, R.G. Shear connection modelling for column removal analysis. *J. Constr. Steel Res.* **2016**, *117*, 227–242. [CrossRef]

38. Shen, J.; Astaneh-Asl, A. Hysteresis model of bolted-angle connections. *J. Constr. Steel Res.* **2000**, *54*, 317–343. [CrossRef]

39. Stylianidis, P.M.; Nethercot, D.A.; Izzuddin, B.A.; Elghazouli, A.Y. Progressive collapse: Failure criteria used in engineering analysis. In *Structures Congress 2009: Don't Mess with Structural Engineers: Expanding Our Role*; ASCE: Reston, VA, USA, 2009.

40. *Seismic Provisions for Structural Steel Buildings*; American Institute of Steel Construction: Chicago, IL, USA, 2010.

41. Zhong, W.; Meng, B.; Hao, J. Performance of different stiffness connections against progressive collapse. *J. Constr. Steel Res.* **2017**, *135*, 162–175. [CrossRef]

42. Faridmehr, I.; Osman, M.H.; Tahir, M.B.M.; Nejad, A.F.; Hodjati, R. Seismic and progressive collapse assessment of SidePlate moment connection system. *Struct. Eng. Mech.* **2015**, *54*, 35–54. [CrossRef]

43. Wang, W.; Fang, C.; Qin, X.; Chen, Y.; Li, L. Performance of practical beam-to-SHS column connections against progressive collapse. *Eng. Struct.* **2016**, *106*, 332–347. [CrossRef]

44. Yang, B.; Tan, K.H. Experimental tests of different types of bolted steel beam–column joints under a central-column-removal scenario. *Eng. Struct.* **2013**, *54*, 112–130. [CrossRef]

45. Mckay, A.; Gomez, M.; Marchand, K. *Non-Linear Dynamic Alternate Path Analysis for Progressive Collapse: Detailed Procedures Using UFC 4-023-03*; Protection Engineering Consultants: Castle Hills, TX, USA, 2010; (Revised July 2009).

46. Pekelnicky, R.; Engineers, S.D.; Poland, S.C.; Engineers, N.D. Seismic Evaluation and Retrofit Rehabilitation of Existing Buildings. In Proceedings of the SEAOC, Santa Fe, NM, USA, 12–15 September 2012.

47. Daneshvar, H.; Driver, R.G. Behaviour of shear tab connections in column removal scenario. *J. Constr. Steel Res.* **2017**, *138*, 580–593. [CrossRef]

48. Liu, X.C.; Cui, F.Y.; Zhan, X.X.; Yu, C.; Jiang, Z.Q. Seismic performance of bolted connection of H-beam to HSS-column with web end-plate. *J. Constr. Steel Res.* **2019**, *156*, 167–181. [CrossRef]

49. Kermajani, M.; Ghaini, F.M.; Miresmaeili, R.; AghaKouchak, A.; Shadmand, M. Effect of weld metal toughness on fracture behavior under ultra-low cycle fatigue loading (earthquake). *Mater. Sci. Eng. A* **2016**, *668*, 30–37. [CrossRef]